Quest: Journal of Geometry, Mathematical and Quantum Physics (Quest)
e-ISSN: 3064-7282 Vol.3 Issue 9|2026

Design and Optimization of Polarization-Insensitive Broadband Antireflection Coating for MWIR Windows Using ZEMAX

Hussein T. Hashim[1]*, Hadeel T. Hashim[2], Ali H. Al-Hamdani [3,4], Mohammad A.R. Hussein[3], Anwer S. Aljuboury[5,6]
1,2 Ministry of Education Iraq/ General Directorate of Education in Al-Qādisiyyah Governorate, Iraq.
3 Gilgamesh University, College of Science, Baghdad, Iraq.
4 Department of Laser and Optoelectronic Engineering, University of Technology, Iraq
5 Gilgamesh University, Baghdad, Iraq
6 Al-Mustansirya University, Baghdad, Iraq.
*Correspondence: ali.h.abdulmuneim@gu.edu.iq

Citation: Hashim, H. T., Hashim, H. T., Al-Hamdani, A. H., Hussein, M. A. R., Aljuboury, A. S. Design and Optimization of Polarization-Insensitive Broadband Antireflection Coating for MWIR Windows Using ZEMAX. Quest: Journal of Geometry, Mathematical and Quantum Physics (Quest) 2026, 3(9), 8-17.

Received: 24th Jul 2026
Revised: 11th Aug 2026
Accepted: 28th Aug 2026
Published: 5th September 2026

Abstract: This study designed and simulated polarization-insensitive broadband anti-reflection coatings (BBARCs) for a middle infrared wavelength (MWIR) window lying between 3 and 5μm, adopting ZEMAX software. BaF_2, MgF_2, ZrO_2, SiO, SiO_2, CdTe, Si, and Y_2O_3 were selected as transparent materials deposited on germanium (Ge), silicon (Si), and zinc selenide (ZnSe). Results show that the reflectance of Ge, Si, and ZnSe substrates reduced from (36%, 30%, and 16%) to virtual null reflectance over a wide angular range. ZEMAX software was used to reduce reflectance considerably and improve spectral performance. In this work, the optimum design was achieved with layers systematically added to the substrate and only layer thickness varied, keeping the index of refraction fixed.

Keywords: Anti-reflection coatings, multi-layer thin-film, polarization insensitive coating, ZEMAX software, optimization methods

Introduction

Over the years, extensive research and development have been dedicated to anti-reflection coatings (ARCs) for both the infrared (IR) and visible regions, owing to their critical importance and broad applications in the optical industry Park and Lee [1]. ARCs are utilized in a wide range of fields, including IR semiconductor laser and detectors, night vision, communications, solar cells, thermal imaging, defense, rocket systems, and space [2], [3], [4], [5], [6]. ARCs are utilized in therapeutic applications for the human eye that may cause enzyme denaturation due to increased temperature[6], [7]. The performance of AR coatings is significantly enhanced by reducing surface reflections in these applications. In addition to lowering reflection, ARCs play a vital role in increasing transmittance in various optical systems [7]. High-performance AR coatings are particularly essential in advanced applications such as dye lasers and facet laser techniques[8], [9], [10], including external cavity quantum cascade lasers, where they ensure optimal functionality. AR-coated laser facets with low reflectance across a broad wavelength range are critical for achieving wide laser tunability [10], [11], [12], [13]. However, designing high-performance coatings for the infrared region remains a significant challenge due to the limited availability of low-loss materials suitable for these wavelengths [14], [15]. This limitation restricts the selection of materials with suitable refractive indices for designing coatings in the mid-wave and long-wave infrared spectral ranges. Multi-layer coating models provide a pathway to high-performance ARC designs through relatively straightforward computational methods [16]. Recently, Rashid et al. adopted the method of combining thickness and refractive index simultaneously to achieve the optimum design of ARC's coating using ZEMAX software[17]. The optimization process enables the design of highly efficient optical coatings, even with a limited selection of materials. In this paper, we present broadband antireflection coatings that operate across the $(3-5\,\mu m)$ wavelength range and oblique angles of incidence, with a central design wavelength of $4\,\mu m$. The AR-coating architecture was further optimized by implementing a practical refractive index approach, which reduced the overall stack thickness.

Theory

The most uncomplicated AR-coating design is a single layer deposited on a substrate [18], it requires a layer index of refractive to satisfy the reflection-less condition:

$$n_1 = \sqrt{n_s\, n_0} \quad (1),$$

Where "$n_1,\ n_s\ \&\ n_0$" are the refractive index of the single layer, substrate, and air, respectively. The refractive index (n) of a medium relative to the state of polarization of the radiation passing through it. Specifically, for the two linearly polarized components $p\,(TM-mode)$ and $s\,(TE-mode)$, we have[19]:

$$\eta_p = n/cos\theta \quad (2),$$

$$\eta_s = ncos\theta, \quad (3),$$

"n" is the nominal refractive index of the layer; "θ" is the angle at which light passes through the layer, which corresponds to the angle of refraction determined by Snell's law. $n_0 sin\theta_0 = nsin\theta$.

Characteristic matrices are commonly employed to calculate the reflectance of an assembly of thin-film layers, which is already included with ZEMAX software[20]. A 2×2 matrix represents each layer is referred to as the "characteristic matrix" of the thin film [21]:

$$M_j = \begin{pmatrix} cos\delta_r & (isin\delta_r)/\eta_r \\ i\eta_r sin\delta_r & cos\delta_r \end{pmatrix} \quad (4),$$

Where η_r represents the "effective refractive index" of the layer, and δ_r denotes its "phase thickness" given by:

$$\delta_r = 2\pi n_r\, d_j \cos\theta_r/\lambda \quad (5),$$

Where d_j is the "optical phase thickness" of the j^{th} sub-layer, and λ is the wavelength of the incident light beam.

According to the refractive index and thickness of each layer, the reflectance for the multilayer assembly calculated by [19]:

$$\begin{bmatrix} B \\ C \end{bmatrix} = \left\{ \prod_{r=1}^{q} \begin{bmatrix} cos\delta_r & (isin\delta_r)/\eta_r \\ i\eta_r sin\delta_r & cos\delta_r \end{bmatrix} \right\} \begin{bmatrix} 1 \\ \eta_{Sub} \end{bmatrix} \quad (6),$$

Where $B\ and\ C$ represent the total electric $(s-polarized)$ and magnetic $(p-polarized)$ field amplitudes of the light propagating in the medium, respectively. The optical admittance is defined as [22]:

$$Y = \frac{C}{B} \quad (7),$$

The reflectance of a quarter -wave stacks at oblique incidence, according to the Fresnel equation in air [23], [24] are given by:

$$R = \left(\frac{\eta_0 B - C}{\eta_0 B + C}\right)\left(\frac{\eta_0 B - C}{\eta_0 B + C}\right)^* \quad (8),$$

Where the brackets consist of real and imaginary components, respectively. The layer thickness was changed from operand "CODA" which constrains the coating multiplier. An extensive search for the optimal solution was conducted using ZEMAX, enriched with a merit function of the least squares method [20]:

$$MF = \left[\frac{\sum W_i (V_i - T_i)^2}{\sum W_i}\right]^{1/2} \quad (9),$$

Where W, V, and T denote the "weight of the operand," "current," and" target" values (the absolute value), and $"i"$ indicates the operand number.

Materials and Methods

Materials and Design Configuration

Germanium (Ge), silicon (Si), and zinc selenide (ZnSe) were selected as MWIR window substrates with refractive indices of 4.00, 3.14, and 2.43, respectively [25]. The target spectral interval was 3–5 µm, with a design wavelength of 4 µm. Reflectance was evaluated at normal incidence and across oblique incidence angles.
The candidate antireflection-film materials were BaF2, MgF2, ZrO2, SiO, SiO2, CdTe, Si, and Y2O3. Their refractive indices were taken as 1.30, 1.38, 2.05, 1.60, 1.40, 2.64, 3.42, and 1.73, respectively, consistent with the optical materials described in the original study [7], [26]. During optimization, the refractive indices were kept fixed and layer thicknesses were treated as the principal design variables.

ZEMAX Modeling and Optimization Procedure

The coating design was developed progressively from single-layer to two-, three-, and four-layer stacks. ZEMAX was used to implement the characteristic-matrix calculation and the least-squares merit function described in Section 2 [20]. Quarter-wave optical thickness served as the initial condition, after which Hammer optimization was used to vary thickness and to grow, remove, or rearrange layers until broadband reflectance in the 3–5 µm region was minimized.

Results

Layer-by-Layer Reflectance Reduction

The preliminary multilayer models produced a consistent reduction in maximum reflectance as the number of layers increased. For Ge, the maximum reflectance decreased from about 36% for the bare substrate to 9.85%, 3.73%, 3.11%, and 2.50% for the single-, two-, three-, and four-layer designs, respectively. For Si, the corresponding values were 8.19%, 2.52%, 1.84%, and 1.51%, while ZnSe reached 4.22%, 2.49%, 1.63%, and 1.13%. Tables 1–3 summarize the optimized layer materials and thicknesses for each substrate.

Table 1. Design data and reflectance values for all configurations on the Ge substrate.

Configurations	Material	Refractive Index (n) at $\lambda_0 = 4\ \mu m$	Thickness (μm)	Max - R_{ave}(%) for (3- 5µm) region
Single Layer	ZrO_2	2.05	0.2412	9.85
Two-Layers	SiO CdTe	1.60 2.64	0.2459 0.2425	3.73
Three-Layers	SiO CdTe Si	1.60 2.64 3.42	0.2412 0.2354 0.2324	3.11
Four-Layers	BaF_2 ZrO_2 CdTe Si	1.30 2.05 2.64 3.42	0.2408 0.2475 0.2150 0.2351	2.50

Table 2. Design data and reflectance values for all configurations on the Si substrate.

Configurations	Material	Refractive Index (n)	Thickness (μm)	Max - R_{ave}(%)

		at $\lambda_0 = 4\ \mu m$		for (3- 5μm) region
Single Layer	Y_2O_3	1.73	0.2426	8.19
Two- Layers	BaF_2 $CdTe$	1.30 2.64	0.2394 0.2409	2.52
Three- Layers	MgF_2 ZrO_2 $CdTe$	1.38 2.05 2.64	0.2254 0.1535 0.1951	1.84
Four- Layers	MgF_2 $ZnSe$ MgF_2 $ZnSe$	1.30 2.39 2.64 2.39	0.2271 0.0344 0.0428 0.2492	1.51

Table 3. Design data and reflectance values for all configurations on the ZnSe substrate.

Configurations	Material	Refractive Index (n) at $\lambda_0 = 4\ \mu m$	Thickness (μm)	Max - R_{ave}(%) for (3- 5μm) region
Single Layer	Y_2O_3	1.73	0.2376	4.22
Two- Layers	BaF_2 Y_2O_3	1.30 1.73	0.2429 0.2375	2.49
Three- Layers	BaF_2 Y_2O_3 ZrO_2	1.38 1.73 2.05	0.2350 0.2350 0.2925	1.63
Four- Layers	SiO_2 ZrO_2 Y_2O_3 ZrO_2	1.40 2.05 1.73 2.05	0.2405 0.4772 0.2425 0.2500	1.13

Finally, from Fig.1 and Tables 1-3, it is clear now that the reflectance decreases from ~9% to around 1%, altogether decreasing in bandwidth to 400nm for Ge and Si to 600nm for ZnSe.

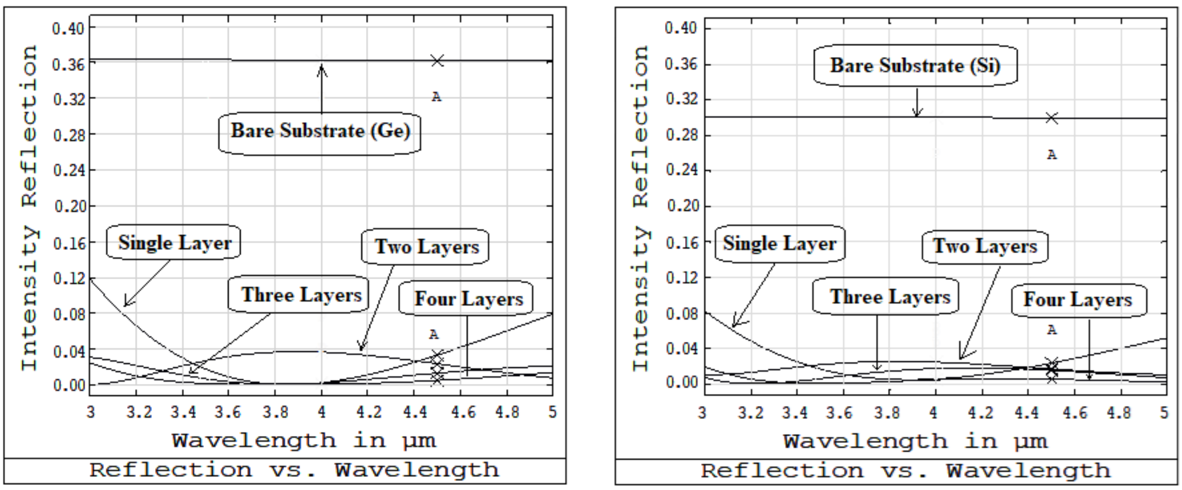

(a) (b)

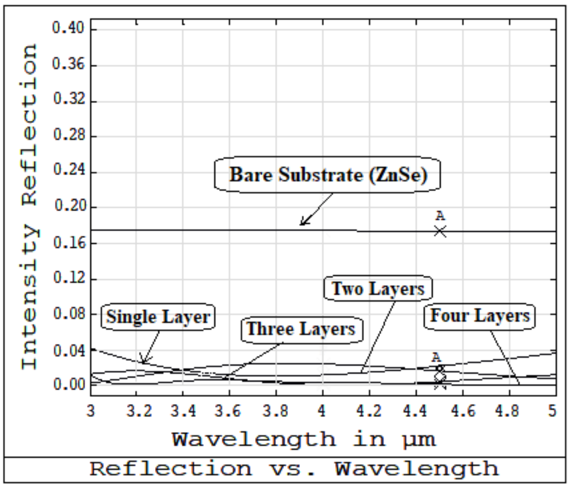

(c)

Figure 1. Combined reflectance profiles of all four configurations designs (single, double, three, and four) layer ARC's on (a) Ge substrate, (b) Si substrate, (c) ZnSe substrate at $\lambda_0 = 4\,\mu m$.

Optimized Multilayer Performance

Using the procedure described in Section 3, ZEMAX refined the initial multilayer constructions by optimizing quarter-wave optical thicknesses while preserving the practical refractive-index set. The triplet and quartic stacks were evaluated over the complete 3–5 µm MWIR band.

The initial configurations in Fig. 1 were subsequently subjected to Hammer optimization. The final optimized three- and four-layer designs for Ge, Si, and ZnSe are presented in Figs. 2–4, while Table 4 summarizes their residual reflectance. The layer constructions retained the quarter-wave optical-thickness framework and were selected to minimize broadband reflection.

1 Model 1: Three layers:

- ❖ Air 1.00 | 1.30 $0.1638\lambda_0$ | 1.60 $0.1150\lambda_0$ | 2.64 $0.2186\lambda_0$ | Ge 4.00
- ❖ Air 1.00 | 1.30 $0.2153\lambda_0$ | 2.05 $0.1522\lambda_0$ | 2.64 $0.1509\lambda_0$ | Si 3.14
- ❖ Air 1.00 | 1.30 $0.2090\lambda_0$ | 1.73 $0.1005\lambda_0$ | 2.05 $0.1818\lambda_0$ | ZnSe 2.43

2 Model 2: Four layers:

- ❖ Air 1.00 | 1.30 $0.2003\lambda_0$ | 2.05 $0.1603\lambda_0$ | 2.64 $0.0894\lambda_0$ | 3.42 $0.1742\lambda_0$ | Ge 4.00
- ❖ Air 1.00 | 1.30 $0.1979\lambda_0$ | 2.05 $0.0828\lambda_0$ | 1.30 $0.0306\lambda_0$ | 2.64 $0.2119\lambda_0$ | Si 3.14
- ❖ Air 1.00 | 1.30 $0.2114\lambda_0$ | 1.73 $0.0864\lambda_0$ | 2.05 $0.2119\lambda_0$ | 2.64 $0.0462\lambda_0$ | ZnSe 2.43

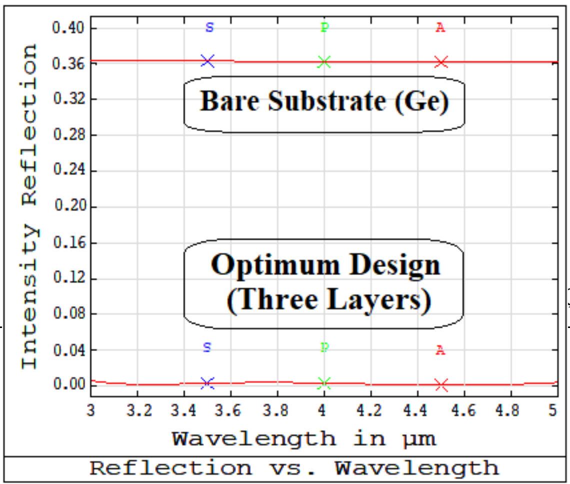

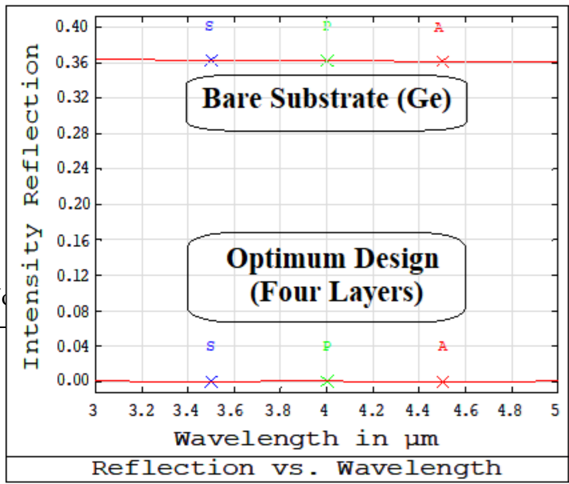

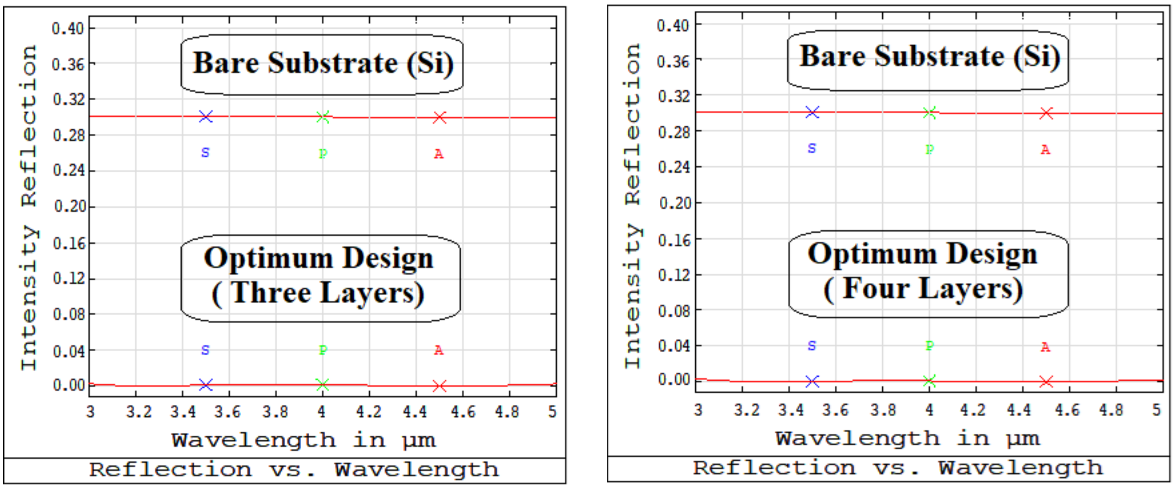

(a) (b)

Figure 3. Reflectance *vs.* wavelength of the ARC's optimum design on Si for: (a) 3-layers, (b) 4-layers, at normal incidence and $\lambda_0 = 4\,\mu m$.

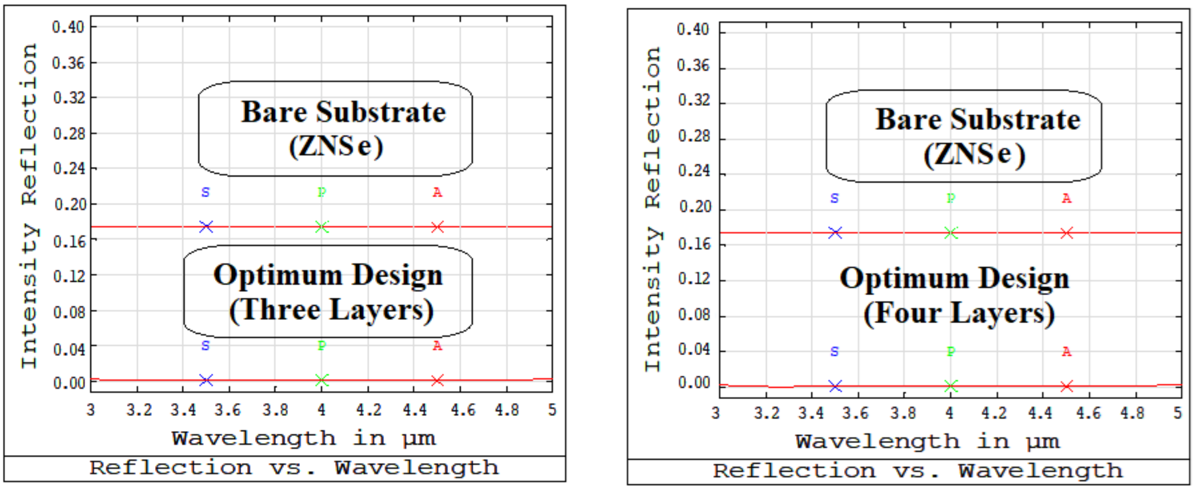

(a) (b)

Figure 4. Reflectance *vs.* wavelength of the ARC's optimum design on ZnSe for: (a) 3-layers, (b) 4-layers, at normal incidence and $\lambda_0 = 4\,\mu m$.

Figs. (2-4) Despite the optimum reflectance behavior for the proposed multilayer design, adding layers will increase software flexibility to arrive quickly at the desired reflectance value. Table 4 summarizes the obtained results.

Table 4. Optimum reflectance for triplet and quartic layers deposited on (Ge, Si, and ZnSe) substrate.

Substrate	$R(\%) at\ \lambda_0 = 4\mu m$	
	Triplet	Quartic
Ge	~ 0.55	~ 0.15
Si	~ 0.28	~ 0.16
ZnSe	~ 0.21	~ 0.14

Thus, it is show that this optimum design models ZEMAX software has high flexibility and adaptability to design anti-reflective coatings with a significant improvement in reflectance value as well as obtaining a wide bandwidth to around $(2000\,nm)$ and wide angles $\sim 60°$ as shown in Fig. 5.

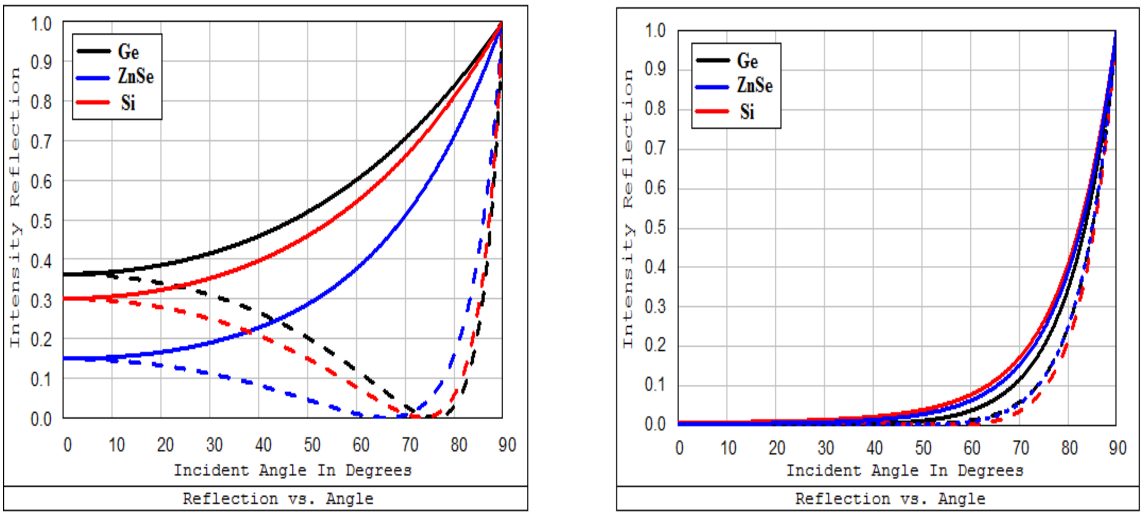

(a) (b)

Figure 5. Reflectance *vs.* angle of incidence of: (a) optimum design of ARC's, (b) Ge, Si, and ZnSe substrates from the air, at the wavelength design (λ_0= 4 μm).

Fig. 5. depicts the variation of the reflectance of bare "Ge, Si, ZnSe" substrates versus the angle of the incident. For normal and near normal incidences, undistinguished in the behavior of two states of polarization, $s-$components (solid), known as an electric field (TE), and $p-$component (dash), known as the magnetic field (TM) were observed.

As the angle of incidence increases, the reflectance for the TM mode (, R_{TM}) drops to zero at the Brewster angle (θ_B). In contrast, the reflectance for the TE mode (R_{TE}) never reaches zero under this condition, resulting in reflected light that consists solely of the TE mode and is linearly polarized. When the angle of incidence approaches grazing incidence (θ ≈ 90°), both R_{TE} and R_{TM} approach unity, meaning nearly all the light is reflected.

Discussion

The results show a clear multilayer-interference effect: increasing the number of dielectric layers progressively suppresses the large Fresnel reflection of the high-index Ge, Si, and ZnSe substrates. The preliminary four-layer designs reduce the maximum reflectance to 2.50% for Ge, 1.51% for Si, and 1.13% for ZnSe. This trend agrees with established multilayer antireflection-coating theory and with computational approaches that use additional design degrees of freedom to broaden the low-reflectance region [9], [16].

The second-stage ZEMAX optimization produces a further substantial improvement. The optimized triplet/quartic reflectance values are approximately 0.55%/0.15% for Ge, 0.28%/0.16% for Si, and 0.21%/0.14% for ZnSe. The relatively small residual reflectance of the quartic stacks indicates that thickness refinement and refractive-index ordering can achieve strong broadband impedance matching without requiring a very large number of layers. This behavior is consistent with the flexibility of numerical optical-coating optimization reported in earlier ZEMAX-based and needle-optimization studies [16], [17], [20].

The angular-response analysis also supports the polarization-insensitive objective over the practical field-of-view region. At normal and near-normal incidence, TE and TM behavior remains similar, whereas the two polarizations separate at larger angles and the TM component approaches zero near the Brewster angle, as expected from Fresnel theory [23], [24]. The reported 3–5 μm bandwidth and approximately 0–60° useful angular range therefore make the optimized stacks promising for MWIR windows. Nevertheless, the present work is simulation-based; fabrication tolerances, wavelength-dependent material dispersion, absorption losses, and environmental durability should be examined experimentally before practical deployment [14], [15].

Conclusion

This article presented a reliable strategy for designing a broadband AR coating with ZEMAX. In this respect, we studied the change of reflectance with wavelength and angle incidence with the change of layers. An algorithm can be developed to achieve an optimal design using numerical optimization, incorporating targets, weights, and layers. This algorithm aims to optimize the design parameters to meet specific performance criteria. The results demonstrate that the design achieves 100% transmission (T=100%) across a broad spectral width of approximately 2000 nm, covering a spectral wavelength range of 3-5 μm and an angular view range of 0-60°. Furthermore, the algorithm remains valid and efficient when applied to the same design structure for other spectral bands centered at different wavelengths, showcasing its versatility and robustness.

Acknowledgment

The authors thank the Ministry of Education Iraq and the University of Gilgamesh, Baghdad-Iraq, for their support in the present work.

REFERENCES

[1] S. Park and Y. Lee, "Design of multilayer antireflection coatings," Journal of the Korean Physical Society, vol. 32, no. 5, pp. 676–680, 1998.

[2] Y. Dogan, İ. Erdogan, and A. Altuntepe, "Design and fabrication of highly efficient antireflective coating in MWIR on germanium using ion-assisted e-beam deposition," Optical Materials, vol. 157, no. 2, Art. no. 116362, 2024.

[3] R. S. Dubey and Y. Venkatesh, "Engineering of Ultra-Violet reflectors by varying alternate layers of Titania/Silica for harmful UV-protection," vol. 49, no. 4, pp. 1–9, 2022.

[4] F. Sh. Zainalabdeem, A. H. Al-Hamdani, A. J. H. Alid, and G. S. Karam, "Improving the performance efficiency of solar panal by using flat mirror concentrators," AIP Conference Proceedings, vol. 2190, 2019.

[5] A. H. Al-Hamdani, "Z-scan measurements of optical nonlinearities for (3GO) dye," International Journal of Nanoelectronics and Materials Science, vol. 6, p. 139, 2013.

[6] Z. S. Alshaikhli, A. H. Al-Hamdani, E. M. Abbas, S. M. Lafta, and W. A. Hekmat, "Effect of environmental temperature on the performance of different contact lenses materials," Journal of Optics, vol. 51, no. 4, 2023.

[7] A. N. Abd AL-Gaffar, "Java Applet Technology for Design Interference Optical Coating," Baghdad Science Journal, vol. 8, pp. 495–502, 2011.

[8] A. H. Al-Hamdani, H. G. Rashid, and H. T. Hashim, "Optimum design of the hybrid (diffractive/refractive) multifocal intraocular lenses implanted within human eye," Kuwait Journal of Science, vol. 48, no. 1, pp. 59–66, 2021.

[9] M. Asghar, M. Khan, and S. Naseem, "Modeling high performance multilayer antireflection coatings for visible and infrared (3–5 μm) substrates," Semiconductor Physics, Quantum Electronics & Optoelectronics, vol. 6, no. 4, pp. 508–513, 2003.

[10] A. H. Al-Hamdani, S. M. Jasim, E. M. Abbas, D. A. Hassan, and M. M. Jaber, "Spectral properties of hybrid of Rhodamine (6G) dyes doped epoxy resin dissolved in chloroform," Baghdad Science Journal, vol. 16, no. 3, pp. 764–769, 2019.

[11] A. H. Al-Hamdani, A. S. Al-Ethawi, and R. Jabor, "Study the effect of solvent on the optical properties performance of active polymeric laser media," Baghdad Science Journal, vol. 4, no. 3, pp. 387–392, 2007.

[12] A. Wittmann, A. Hugi, E. Gini, N. Hoyler, and J. Faist, "Heterogeneous high-performance quantum-cascade laser sources for broad-band tuning," IEEE Journal of Quantum Electronics, vol. 44, no. 11, pp. 1083–1088, 2008.

[13] J. Kischkat, M. P. Semtsiv, M. Elagin, G. Monastyrskyi, Y. Flores, et al., "Alignment-stabilized interference filter-tuned external-cavity quantum cascade laser," Optics Letters, vol. 39, no. 23, pp. 6561–6564, 2014.

[14] J. D. T. Kruschwitz and W. T. Pawlewicz, "Optical and durability properties of infrared

transmitting thin films," Applied Optics, vol. 36, no. 10, pp. 2157–2159, 1997.
[15] P. Black and J. Wales, "Materials for use in the fabrication of infrared interference filters," Infrared Physics, vol. 8, pp. 209–222, 1968.
[16] A. Tikhonravov, M. Trubetskov, and G. DeBell, "Optical coating design approaches based on the needle optimization technique," Applied Optics, vol. 46, no. 5, pp. 704–710, 2007.
[17] H. G. Rashid, K. A. Mishjil, H. T. Hassim, A. N. Abd Algaffar, and N. F. Habubi, "Design and evaluation of homogeneously mixed dielectric antireflection coatings with ZEMAX," Journal of Physics: Conference Series, vol. 1963, no. 1, Art. no. 012045, 2021.
[18] J. Cox, "Physics of thin films," in Physics of Thin Films, G. Hass and R. E. Thun, Eds. New York, NY, USA: Academic Press, vol. 2, pp. 55–56, 1968.
[19] H. A. Macleod, Thin-Film Optical Filters, 4th ed. London, U.K.: CRC Press/Institute of Physics Publishing, 2010.
[20] Zemax LLC, Zemax 13 Optical Design Program User's Manual, 2014.
[21] J. F. Snell, W. G. Driscoll, and W. Vaughan, Handbook of Optics, vol. I. New York, NY, USA: McGraw-Hill, pp. 8–10, 1978.
[22] Z. Knittl, Optics of Thin Films. New York, NY, USA: Wiley, 1976.
[23] M. Born and E. Wolf, Principles of Optics: Electromagnetic Theory of Propagation, Interference and Diffraction of Light. New York, NY, USA: Cambridge University Press, pp. 491–554, 1999.
[24] I. Popescu, Macroscopic Electromagnetic Theory of Light. Bucharest, Romania: Scientific and Encyclopedic Publishing, 1986.
[25] W. J. Tropf, M. E. Thomas, and T. J. Harris, "Properties of crystals and glasses," in Handbook of Optics, vol. 2, 1995, pp. 33–61.
[26] E. Atad-Ettedgui and S. D'Odorico, "Specialized optical developments in astronomy," Proc. SPIE, vol. 4842, pp. 1–9, 2003.